Available online at www.sciencedirect.com
SCIENCE DIRECT®
Journal of Sound and Vibration 272 (2004) 657–673
JOURNAL OF SOUND AND VIBRATION
www.elsevier.com/locate/jsvi

Influence coefficients on rotor having thick shaft elements and resilient bearings

Oh Sung Jun*

Department of Mechanical Engineering, Jeonju University, Jeonju 560-759, South Korea

Received 13 March 2001; accepted 11 April 2003

Abstract

Timoshenko beam theory is introduced for modelling the behavior of shaft. Complex variables are used to represent the displacement, slope, moment and shear force, and the complex transfer matrix between the variables at both ends of the shaft element is derived and the influence coefficients are analytically derived for the general flexible rotor having two resilient bearings at both ends. Modelling and derivation of the influence coefficients are based on the transfer matrix method. Simulated influence coefficients are compared to the results using the finite element method based on Timoshenko beam theory. Simulation of the influence coefficients could suggest the guideline for determining the positions of the balancing and measuring planes and the running speed.

1. Introduction

According to which analysis tool is used, a beam theory is limitedly adopted. In modelling a thick shaft for rotor analysis Timoshenko beam theory is commonly introduced when using the finite element method. Because of the feature of the method, however, the calculated results have some error [1]. On the other hand, the transfer matrix method is a technique giving the continuities (at the stations) to the parameters satisfying the equations of motion. Thus if a proper theory, that is, the Timoshenko beam theory, is adopted, the exact results such as the exact natural frequencies and the corresponding modes, which are continuous, are likely to be obtained.

Jun and Kim [1] have derived the analytic expression for the elastodynamic behavior of a rotating thick shaft, and developed a method analyzing the natural vibrations for multi-step rotating shaft. In that method, the analytic expression for a uniform shaft is considered to satisfy the continuity conditions at the boundary where the cross-section changes. The method, however,

*Tel.: +82-63-220-2614; fax: +86-63-220-2750.
E-mail address: junos@jeonju.ac.kr (O.S. Jun).

0022-460X/03/$ - see front matter
doi:10.1016/S0022-460X(03)00393-6

has limitation in application to the model having disks. Based on the analytic expression of the method, the author of this paper derives the transfer matrix between both the ends of a uniform shaft to extend the application to the model having disks. Using the transfer matrix help us also to expand the idea to the forced response analyses on rotors.

Influence coefficient is a transfer function on rotor, which is one of the tools used in rotor balancing [2–4]. Influence coefficients are generally obtained by attaching trial masses on the balancing planes of a rotor and by measuring the corresponding responses. They are also calculated from the finite element method. In this study, the influence coefficients are analytically derived for the general flexible rotor. Modelling and derivation of the influence coefficients are based on the transfer matrix method.

2. Transfer matrix

2.1. Equation of motion

The elastodynamic behavior of a thick uniform shaft is described by considering the rotary inertia and shear deformation of the cross-section. Especially for rotating shaft, the gyroscopic effect due to the rotation is also considered. Including the torque in a power-transmitting shaft, and introducing the complex displacement

$$u(x,t) = y(x,t) + \mathrm{j}z(x,t), \tag{1}$$

the equation of motion of the rotating shaft is written as follows [5]:

$$\begin{aligned} &EI\frac{\partial^4 u}{\partial x^4} - \frac{EI\rho}{\kappa G}\frac{\partial^4 u}{\partial x^2 \partial t^2} - \mathrm{j}T\frac{\partial^3 u}{\partial x^3} + \mathrm{j}\frac{T\rho}{\kappa G}\frac{\partial^3 u}{\partial x \partial t^2} + \rho A\frac{\partial^2 u}{\partial t^2} \\ &- \rho A r_0^2\left[\left(\frac{\partial^4 u}{\partial x^2 \partial t^2} - \frac{\rho}{\kappa G}\frac{\partial^4 u}{\partial t^4}\right) - \mathrm{j}2\Omega\left(\frac{\partial^3 u}{\partial x^2 \partial t} - \frac{\rho}{\kappa G}\frac{\partial^3 u}{\partial t^3}\right)\right] = 0, \end{aligned} \tag{2}$$

where x is the axial co-ordinate and y and z are the displacements in the horizontal and vertical directions, respectively. T is the torque on each end of the shaft, and E, G and ρ are Young's modulus, shear modulus and mass density, respectively. A and I are the area and area moment of inertia of the cross-section, r_0 is the radius of gyration, κ is the inverse of the generally used form factor, and Ω is the rotating speed.

The harmonic motion of natural frequency ω can be separated in the variable $u(x,t)$ as

$$u(x,t) = U(x)\mathrm{e}^{\mathrm{j}\omega t}. \tag{3}$$

Substituting Eq. (3) into Eq. (2) results in the following equation:

$$\frac{\mathrm{d}^4 U}{\mathrm{d}x^4} + a\frac{\mathrm{d}^3 U}{\mathrm{d}x^3} + b\frac{\mathrm{d}^2 U}{\mathrm{d}x^2} + c\frac{\mathrm{d}U}{\mathrm{d}x} + \mathrm{d}U = 0, \tag{4}$$

where

$$a = -\frac{\mathrm{j}T}{EI},$$
$$b = \frac{1}{EI}\left[\left(\frac{EI\rho}{\kappa G} + \rho A r_0^2\right)\omega^2 - 2\rho A r_0^2 \Omega\omega\right],$$
$$c = -\mathrm{j}\frac{1}{EI}\frac{T\rho}{\kappa G}\omega^2,$$
$$d = \frac{1}{EI}\left[\frac{\rho^2 A r_0^2}{\kappa G}\omega^4 - 2\frac{\rho^2 A r_0^2 \Omega}{\kappa G}\omega^3 - \rho A\omega^2\right]. \tag{5}$$

Using the four roots of the polynomial [1,6], the solution of Eq. (4) is expressed as

$$U = p_1 \mathrm{e}^{\lambda_1 x} + p_2 \mathrm{e}^{\lambda_2 x} + p_3 \mathrm{e}^{\lambda_3 x} + p_4 \mathrm{e}^{\lambda_4 x}. \tag{6}$$

Eq. (6) means that the elastodynamic behavior of the rotating shaft is dependent on λ's, which are determined by several parameters, such as rotating speed Ω, natural frequency ω, and geometric and material properties of the shaft. The coefficients p_1, p_2, p_3, p_4 of Eq. (6) are also complex values defined in a uniform shaft segment[1].

2.2. Complex state variable

Figs. 1 and 2 show the state variables on ith element in $X-Z$ and $X-Y$ planes, respectively. Introducing the complex quantities yields the complex state variables as follows:

$$U_i = Y_i + \mathrm{j}Z_i,$$
$$\alpha_i = \phi_i + \mathrm{j}\theta_i,$$
$$M_i = M_{z,i} + \mathrm{j}M_{y,i},$$
$$V_i = V_{y,i} + \mathrm{j}V_{z,i}. \tag{7}$$

The slope α, moment M and shear force V have the following relations [5]:

$$\alpha = \frac{\mathrm{d}U}{\mathrm{d}x},$$

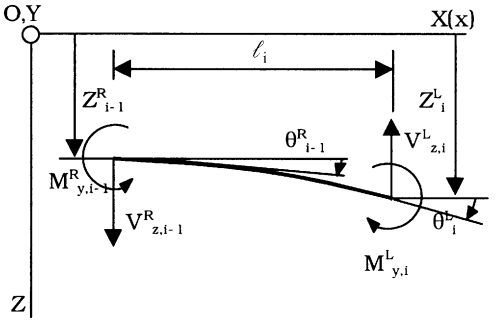

Fig. 1. State variables of ith element in X–Z plane.

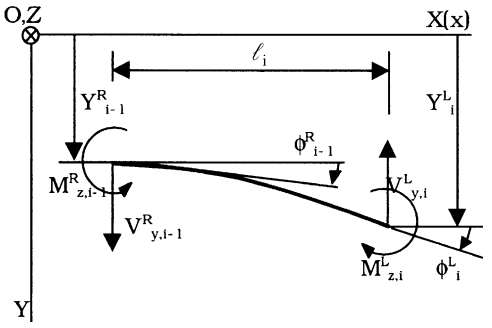

Fig. 2. State variables of ith element in X–Y plane.

$$M = EI\frac{\mathrm{d}^2U}{\mathrm{d}x^2} - \mathrm{j}T\frac{\mathrm{d}U}{\mathrm{d}x},$$

$$V = EI\frac{\mathrm{d}^3U}{\mathrm{d}x^3} - \mathrm{j}T\frac{\mathrm{d}^2U}{\mathrm{d}x^2} + \rho Ar_0^2(\omega^2 - 2\omega\Omega)\frac{\mathrm{d}U}{\mathrm{d}x}. \tag{8}$$

2.3. Transfer matrix of shaft element

The state variables at $x = 0$, i.e., at the left-hand side of shaft element, are expressed from Eqs. (6) and (8) as follows:

$$\begin{aligned} U_0 &= p_1 + p_2 + p_3 + p_4, \\ \alpha_0 &= \lambda_1 p_1 + \lambda_2 p_2 + \lambda_3 p_3 + \lambda_4 p_4, \\ M_0 &= g_1 p_1 + g_2 p_2 + g_3 p_3 + g_4 p_4, \\ V_0 &= h_1 p_1 + h_2 p_2 + h_3 p_3 + h_4 p_4, \end{aligned} \tag{9}$$

where

$$\begin{aligned} g_1 &= EI\lambda_1^2 - \mathrm{j}T\lambda_1, \quad g_2 = EI\lambda_2^2 - \mathrm{j}T\lambda_2, \\ g_3 &= EI\lambda_3^2 - \mathrm{j}T\lambda_3, \quad g_4 = EI\lambda_4^2 - \mathrm{j}T\lambda_4, \\ h_1 &= EI\lambda_1^3 + \rho Ar_0^2(\omega^2 - 2\omega\Omega)\lambda_1 - \mathrm{j}T\lambda_1^2, \\ h_2 &= EI\lambda_2^3 + \rho Ar_0^2(\omega^2 - 2\omega\Omega)\lambda_2 - \mathrm{j}T\lambda_2^2, \\ h_3 &= EI\lambda_3^3 + \rho Ar_0^2(\omega^2 - 2\omega\Omega)\lambda_3 - \mathrm{j}T\lambda_3^2, \\ h_4 &= EI\lambda_4^3 + \rho Ar_0^2(\omega^2 - 2\omega\Omega)\lambda_4 - \mathrm{j}T\lambda_4^2. \end{aligned} \tag{10}$$

Expressing the coefficients p_1, p_2, p_3, p_4 in terms of U_0, α_0, M_0, V_0 from Eq. (9) and substituting them into the expressions of U_l, α_l, M_l, V_l at $x = l$, the relation between state vectors of each side

of shaft element having length l is written as follows:

$$\begin{pmatrix} U_l \\ \alpha_l \\ M_l \\ V_l \end{pmatrix} = \frac{1}{\Delta}\begin{bmatrix} a_{11} & a_{12} & a_{13} & a_{14} \\ a_{21} & a_{22} & a_{23} & a_{24} \\ a_{31} & a_{32} & a_{33} & a_{34} \\ a_{41} & a_{42} & a_{43} & a_{44} \end{bmatrix}\begin{pmatrix} U_0 \\ \alpha_0 \\ M_0 \\ V_0 \end{pmatrix}, \tag{11}$$

where

$$\Delta = \begin{vmatrix} 1 & 1 & 1 & 1 \\ \lambda_1 & \lambda_2 & \lambda_3 & \lambda_4 \\ g_1 & g_2 & g_3 & g_4 \\ h_1 & h_2 & h_3 & h_4 \end{vmatrix}, \quad a_{11} = \begin{vmatrix} e^{\lambda_1 l} & e^{\lambda_2 l} & e^{\lambda_3 l} & e^{\lambda_4 l} \\ \lambda_1 & \lambda_2 & \lambda_3 & \lambda_4 \\ g_1 & g_2 & g_3 & g_4 \\ h_1 & h_2 & h_3 & h_4 \end{vmatrix},$$

$$a_{12} = \begin{vmatrix} 1 & 1 & 1 & 1 \\ e^{\lambda_1 l} & e^{\lambda_2 l} & e^{\lambda_3 l} & e^{\lambda_4 l} \\ g_1 & g_2 & g_3 & g_4 \\ h_1 & h_2 & h_3 & h_4 \end{vmatrix}, \quad a_{13} = \begin{vmatrix} 1 & 1 & 1 & 1 \\ \lambda_1 & \lambda_2 & \lambda_3 & \lambda_4 \\ e^{\lambda_1 l} & e^{\lambda_2 l} & e^{\lambda_3 l} & e^{\lambda_4 l} \\ h_1 & h_2 & h_3 & h_4 \end{vmatrix},$$

$$a_{14} = \begin{vmatrix} 1 & 1 & 1 & 1 \\ \lambda_1 & \lambda_2 & \lambda_3 & \lambda_4 \\ g_1 & g_2 & g_3 & g_4 \\ e^{\lambda_1 l} & e^{\lambda_2 l} & e^{\lambda_3 l} & e^{\lambda_4 l} \end{vmatrix}, \quad a_{21} = \begin{vmatrix} \lambda_1 e^{\lambda_1 l} & \lambda_2 e^{\lambda_2 l} & \lambda_3 e^{\lambda_3 l} & \lambda_4 e^{\lambda_4 l} \\ \lambda_1 & \lambda_2 & \lambda_3 & \lambda_4 \\ g_1 & g_2 & g_3 & g_4 \\ h_1 & h_2 & h_3 & h_4 \end{vmatrix},$$

$$a_{22} = \begin{vmatrix} 1 & 1 & 1 & 1 \\ \lambda_1 e^{\lambda_1 l} & \lambda_2 e^{\lambda_2 l} & \lambda_3 e^{\lambda_3 l} & \lambda_4 e^{\lambda_4 l} \\ g_1 & g_2 & g_3 & g_4 \\ h_1 & h_2 & h_3 & h_4 \end{vmatrix}, \quad a_{23} = \begin{vmatrix} 1 & 1 & 1 & 1 \\ \lambda_1 & \lambda_2 & \lambda_3 & \lambda_4 \\ \lambda_1 e^{\lambda_1 l} & \lambda_2 e^{\lambda_2 l} & \lambda_3 e^{\lambda_3 l} & \lambda_4 e^{\lambda_4 l} \\ h_1 & h_2 & h_3 & h_4 \end{vmatrix},$$

$$a_{24} = \begin{vmatrix} 1 & 1 & 1 & 1 \\ \lambda_1 & \lambda_2 & \lambda_3 & \lambda_4 \\ g_1 & g_2 & g_3 & g_4 \\ \lambda_1 e^{\lambda_1 l} & \lambda_2 e^{\lambda_2 l} & \lambda_3 e^{\lambda_3 l} & \lambda_4 e^{\lambda_4 l} \end{vmatrix}, \quad a_{31} = \begin{vmatrix} g_1 e^{\lambda_1 l} & g_2 e^{\lambda_2 l} & g_3 e^{\lambda_3 l} & g_4 e^{\lambda_4 l} \\ \lambda_1 & \lambda_2 & \lambda_3 & \lambda_4 \\ g_1 & g_2 & g_3 & g_4 \\ h_1 & h_2 & h_3 & h_4 \end{vmatrix},$$

$$a_{32} = \begin{vmatrix} 1 & 1 & 1 & 1 \\ g_1 e^{\lambda_1 l} & g_2 e^{\lambda_2 l} & g_3 e^{\lambda_3 l} & g_4 e^{\lambda_4 l} \\ g_1 & g_2 & g_3 & g_4 \\ h_1 & h_2 & h_3 & h_4 \end{vmatrix}, \quad a_{33} = \begin{vmatrix} 1 & 1 & 1 & 1 \\ \lambda_1 & \lambda_2 & \lambda_3 & \lambda_4 \\ g_1 e^{\lambda_1 l} & g_2 e^{\lambda_2 l} & g_3 e^{\lambda_3 l} & g_4 e^{\lambda_4 l} \\ h_1 & h_2 & h_3 & h_4 \end{vmatrix},$$

$$a_{34}=\begin{vmatrix} 1 & 1 & 1 & 1 \\ \lambda_1 & \lambda_2 & \lambda_3 & \lambda_4 \\ g_1 & g_2 & g_3 & g_4 \\ g_1 e^{\lambda_1 l} & g_2 e^{\lambda_2 l} & g_3 e^{\lambda_3 l} & g_4 e^{\lambda_4 l} \end{vmatrix}, \quad a_{41}=\begin{vmatrix} h_1 e^{\lambda_1 l} & h_2 e^{\lambda_2 l} & h_3 e^{\lambda_3 l} & h_4 e^{\lambda_4 l} \\ \lambda_1 & \lambda_2 & \lambda_3 & \lambda_4 \\ g_1 & g_2 & g_3 & g_4 \\ h_1 & h_2 & h_3 & h_4 \end{vmatrix},$$

$$a_{42}=\begin{vmatrix} 1 & 1 & 1 & 1 \\ h_1 e^{\lambda_1 l} & h_2 e^{\lambda_2 l} & h_3 e^{\lambda_3 l} & h_4 e^{\lambda_4 l} \\ g_1 & g_2 & g_3 & g_4 \\ h_1 & h_2 & h_3 & h_4 \end{vmatrix}, \quad a_{43}=\begin{vmatrix} 1 & 1 & 1 & 1 \\ \lambda_1 & \lambda_2 & \lambda_3 & \lambda_4 \\ h_1 e^{\lambda_1 l} & h_2 e^{\lambda_2 l} & h_3 e^{\lambda_3 l} & h_4 e^{\lambda_4 l} \\ h_1 & h_2 & h_3 & h_4 \end{vmatrix},$$

$$a_{44}=\begin{vmatrix} 1 & 1 & 1 & 1 \\ \lambda_1 & \lambda_2 & \lambda_3 & \lambda_4 \\ g_1 & g_2 & g_3 & g_4 \\ h_1 e^{\lambda_1 l} & h_2 e^{\lambda_2 l} & h_3 e^{\lambda_3 l} & h_4 e^{\lambda_4 l} \end{vmatrix}.$$

Eq. (11) is rewritten using the vectors and matrix in a simple form

$$\{s\}_{i+1}^{L}=[F]_i\{s\}_i^{R}, \tag{12}$$

where $[F]_i$ is the transfer matrix of the ith shaft element. $\{s\}$ is the complex state vector, subscript i of the state vector is the node number, and superscript L and R denote the left- and right-hand sides of the node, respectively. The state vectors are shown below in detail

$$\{s\}_{i+1}^{L}=\begin{pmatrix} U_{i+1} \\ \alpha_{i+1} \\ M_{i+1} \\ V_{i+1} \end{pmatrix}^{L}, \quad \{s\}_i^{R}=\begin{pmatrix} U_i \\ \alpha_i \\ M_i \\ V_i \end{pmatrix}^{R}. \tag{13}$$

2.4. Transfer matrix at station

2.4.1. Unbalance effect

Fig. 3 shows node i viewed in $Y-Z$ plane. The unbalance is defined as $m_i e_i$ and makes an angle β_i in $\bar{Y}-\bar{Z}$ co-ordinates fixed on the rotor.

Considering the damping force, which is assumed to be proportional to the velocity of the disk center, and the synchronous circular whirl ($\omega=\Omega$), and introducing the complex variable yields

$$V_i^R=V_i^L+m_i\omega^2U_i^{(L)}-\mathrm{j}c\omega U_i^{(L)}+m_ie_i\Omega^2e^{\mathrm{j}(\Omega t+\beta_i)}. \tag{14}$$

2.4.2. Gyroscopic effect

Fig. 4 shows a disk under precession. In the figure, θ and ϕ denote the rotation angles along the Y- and Z-axis, respectively. The spin speed Ω corresponds to the whirl speed in the case of synchronous whirl. The gyroscopic effect of a disk is included.

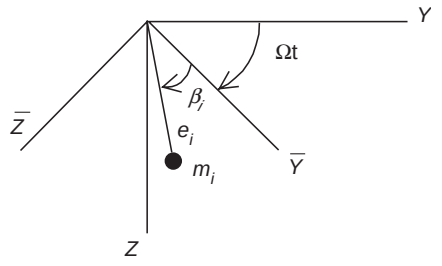

Fig. 3. Unbalance mass at node i

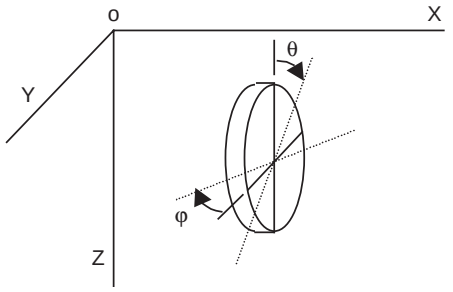

Fig. 4. Disk under precession.

For the synchronous circular whirl ($\omega = \Omega$), the moment equilibrium equation becomes

$$M_i^R = M_i^L + (\omega\Omega J_p - \omega^2 J_t)\alpha_i^L, \tag{15}$$

where J_p and J_t stand for the polar and the transverse mass moment of inertia of disk, respectively.

Considering the unbalance and moment effects (including gyroscopic effect) at the disk, the following relation is represented between the both sides of node i:

$$\begin{pmatrix} U_i \\ \alpha_i \\ M_i \\ V_i \end{pmatrix}^R = \begin{bmatrix} 1 & 0 & 0 & 0 \\ 0 & 1 & 0 & 0 \\ 0 & (\omega\Omega J_p - \omega^2 J_t) & 1 & 0 \\ m_i\omega^2 - \mathrm{j}c\omega & 0 & 0 & 1 \end{bmatrix} \begin{pmatrix} U_i \\ \alpha_i \\ M_i \\ V_i \end{pmatrix}^L + \begin{pmatrix} 0 \\ 0 \\ 0 \\ m_i e_i \Omega^2 \mathrm{e}^{\mathrm{j}(\Omega t + \beta_i)} \end{pmatrix}. \tag{16}$$

2.5. Transfer matrix of resilient support at ends

Bearing support has resilient property. The bearings in this study are assumed to have the equivalent, direct components, $k_{YY} = k_{ZZ}$, only ($k_{YZ} = k_{ZY} = 0$).

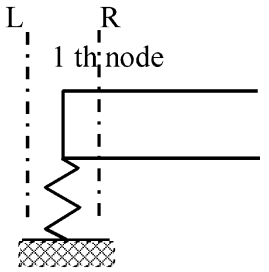

Fig. 5. Resilient support at left end.

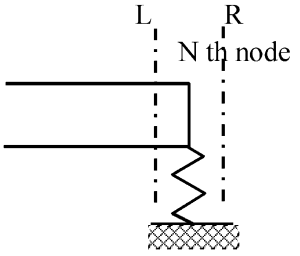

Fig. 6. Resilient support at right end.

Resilient support at left end (Fig. 5)

$$V_1^R = -kU_1^L,$$

where $U_1^L = U_1^R$.

Resilient support at right end

$$0 = V_N^L - kU_N^L,$$

where $U_N^L = U_N^R$ (Fig. 6).

3. Influence coefficient

3.1. Response at measuring point of simple rotor

A simple rotor to calculate the response using the transfer matrixes derived above is shown in Fig. 7. The rotor is mounted on the resilient bearings at nodes 1 and 6. Node numbers 2 and 5 are the measuring planes, 3 and 4 are the balancing planes positioned at both sides of rigid cylinder. The state vectors of the model have the following relations:

$$\begin{aligned}
&\{\ \}_2^M = F^{12}\{\ \}_1^R, \quad \{\ \}_3^L = F^{23}\{\ \}_2^M, \quad \{\ \}_2^R = S^3\{\ \}_3^L + \{\ \}_3, \\
&\{\ \}_4^L = R^{34}\{\ \}_3^R, \quad \{\ \}_4^R = S^4\{\ \}_4^L + \{\ \}_4, \\
&\{\ \}_5^M = F^{45}\{\ \}_4^R, \quad \{\ \}_6^L = F^{56}\{\ \}_5^M,
\end{aligned} \tag{17}$$

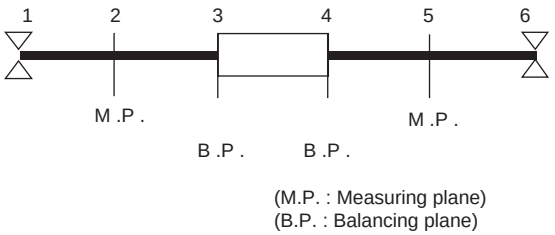

Fig. 7. Rotor model.

where S^i is the transfer matrix between the left- and right-hand sides of balancing plane i, which has form of 4×4 matrix of the right-hand side of Eq. (16). The vector $\{\ \}_i$ indicates the unbalance, which has the fourth element only, on the balancing plane as shown in Eq. (16). $\{\ \}_i^M$ is the state vector on the measuring plane at node i. F^{ij} is the transfer matrix between nodes i and j which are each side of the flexible shaft element.

The matrix R^{34} is the transfer matrix for the massless rigid cylinder, of which mass and moments of inertia are separated into planes 3 and 4 where two disks are assumed. The cylinder can be considered as a mass-distributed thick element. The transfer matrix R^{34} is replaced by F^{34}, and the transfer matrixes S^3 and S^4 are replaced by unit matrix as follows:

$$I=\begin{bmatrix}1&0&0&0\\0&1&0&0\\0&0&1&0\\0&0&0&1\end{bmatrix}.$$

Seven expressions in Eq. (17) are integrated to one equation as follows:

$$\{\ \}_6^L = F^{56}F^{45}S^4R^{34}S^3F^{23}F^{12}\{\ \}_1^R + F^{56}F^{45}S^4R^{34}\{\ \}_3 + F^{56}F^{45}\{\ \}_4. \tag{18}$$

Simplifying this equation using symbols, we have

$$\{\ \}_6^L = T\{\ \}_1^R + Q^{3-6}\{\ \}_3 + Q^{4-6}\{\ \}_4. \tag{19}$$

In Eq. (19), T denotes the transfer matrix between the each end of the entire rotor system, and Q^{3-6} and Q^{4-6} are the transfer matrixes of the balancing planes at node 3 and node 4 to the right-hand side end of rotor, respectively.

Considering the boundary conditions at nodes 1 and 6, the state vectors at nodes are written as

$$\{\ \}_1^R=\begin{Bmatrix}U_1\\ \alpha_1\\ 0\\ -k_1U_1\end{Bmatrix}\quad\text{and}\quad\{\ \}_6^L=\begin{Bmatrix}U_6\\ \alpha_6\\ 0\\ k_6U_6\end{Bmatrix}.$$

From four algebra equations of motion (19), the slope and the shear force at node 1 are expressed as follows:

$$U_1^R = \frac{\begin{vmatrix} -(q_{14}^{3-6}k_6 - q_{44}^{3-6}) & (t_{12}k_6 - t_{42}) \\ -q_{34}^{3-6} & t_{32} \end{vmatrix}}{\begin{vmatrix} (t_{11}k_6 - t_{14}k_1k_6 - t_{41} + t_{44}k_1) & (t_{12}k_6 - t_{42}) \\ (t_{31} - t_{34}k_1) & t_{32} \end{vmatrix}}(m_3e_3\Omega^2 e^{j(\Omega t+\beta_3)}) + \frac{\begin{vmatrix} -(q_{14}^{4-6}k_6 - q_{44}^{4-6}) & (t_{12}k_6 - t_{42}) \\ -q_{34}^{4-6} & t_{32} \end{vmatrix}}{\begin{vmatrix} (t_{11}k_6 - t_{14}k_1k_6 - t_{41} + t_{44}k_1) & (t_{12}k_6 - t_{42}) \\ (t_{31} - t_{34}k_1) & t_{32} \end{vmatrix}}(m_4e_4\Omega^2 e^{j(\Omega t+\beta_4)})$$
$$= c_3^U(m_3e_3\Omega^2 e^{j(\Omega t+\beta_3)}) + c_4^U(m_4e_4\Omega^2 e^{j(\Omega t+\beta_4)}), \tag{20}$$

$$\alpha_1^R = \frac{\begin{vmatrix} (t_{11}k_6 - t_{14}k_1k_6 - t_{41} + t_{44}k_1) & -(q_{14}^{3-6}k_6 - q_{44}^{3-6}) \\ (t_{31} - t_{34}k_1) & -q_{34}^{3-6} \end{vmatrix}}{\begin{vmatrix} (t_{11}k_6 - t_{14}k_1k_6 - t_{41} + t_{44}k_1) & (t_{12}k_6 - t_{42}) \\ (t_{31} - t_{34}k_1) & t_{32} \end{vmatrix}}(m_3e_3\Omega^2 e^{j(\Omega t+\beta_3)}) + \frac{\begin{vmatrix} (t_{11}k_6 - t_{14}k_1k_6 - t_{41} + t_{44}k_1) & -(q_{14}^{4-6}k_6 - q_{44}^{4-6}) \\ (t_{31} - t_{34}k_1) & -q_{34}^{4-6} \end{vmatrix}}{\begin{vmatrix} (t_{11}k_6 - t_{14}k_1k_6 - t_{41} + t_{44}k_1) & (t_{12}k_6 - t_{42}) \\ (t_{31} - t_{34}k_1) & t_{32} \end{vmatrix}}(m_4e_4\Omega^2 e^{j(\Omega t+\beta_4)})$$
$$= c_3^\alpha(m_3e_3\Omega^2 e^{j(\Omega t+\beta_3)}) + c_4^\alpha(m_4e_4\Omega^2 e^{j(\Omega t+\beta_4)}), \tag{21}$$

where q_{ij}^{3-6} and t_{ij} denote the (i,j) element of Q^{3-6} and T matrices, respectively.

Since the state vector at node 2 is $\{\ \}_2^M = F^{12}\{\ \}_1^R$, where

$$\{\ \}_1^R = \begin{Bmatrix} U_1 \\ \alpha_1 \\ 0 \\ -k_1U_1 \end{Bmatrix},$$

the response at the measuring plane of node 2 is

$$U_2 = \{(f_{11}^{12} - f_{14}^{12}k_1)c_3^U + f_{12}^{12}c_3^\alpha\}(m_3e_3\Omega^2 e^{j(\Omega t+\beta_3)}) + \{(f_{11}^{12} - f_{14}^{12}k_1)c_4^U + f_{12}^{12}c_4^\alpha\}(m_4e_4\Omega^2 e^{j(\Omega t+\beta_4)}). \tag{22}$$

In a similar manner, the response at the measuring plane of node 5 is expressed as

$$U_5 = \{(q_{11}^{1-5} - q_{14}^{1-5}k_1)c_3^U + q_{12}^{1-5}c_3^\alpha + q_{14}^{3-5}\}(m_3e_3\Omega^2 e^{j(\Omega t+\beta_3)}) + \{(q_{11}^{1-5} - q_{14}^{1-5}k_1)c_4^U + q_{12}^{1-5}c_4^\alpha + q_{14}^{4-5}\}(m_4e_4\Omega^2 e^{j(\Omega t+\beta_4)}). \tag{23}$$

The responses at the measuring planes are expressed in a closed form in terms of the unbalances at the balancing planes as shown in Eqs. (22) and (23).

3.2. Generalization of influence coefficient

Fig. 8 shows a general rotor having N nodes with two resilient bearings at both ends. Using relations derived from a simple rotor, the equation of the entire system is written as follows:

$$\{\ \}_N^L = T\{\ \}_1^R + Q^{B1-N}\{\ \}_{B1} + Q^{B2-N}\{\ \}_{B2} + \cdots + Q^{Bi-N}\{\ \}_{Bi} + \cdots, \tag{24}$$

where superscripts and subscripts $B1$, $B2$, …, Bi denote the node number of balancing planes. Considering the boundary conditions for the resilient bearings of stiffness k_L and k_R at nodes 1 and N, respectively, we obtain

$$\begin{aligned} U_1^R &= \sum_{No.(Bi)} \frac{\begin{vmatrix} -(q_{14}^{Bi-N}k_R - q_{44}^{Bi-N}) & (t_{12}k_R - t_{42}) \\ -q_{34}^{Bi-N} & t_{32} \end{vmatrix}}{\begin{vmatrix} (t_{11}k_R - t_{14}k_Lk_R - t_{41} + t_{44}k_L) & (t_{12}k_R - t_{42}) \\ (t_{31} - t_{34}k_L) & t_{32} \end{vmatrix}} (m_{Bi}e_{Bi}\Omega^2 e^{j(\Omega t+\beta_{Bi})}) \\ &= \sum_{No.(Bi)} c_{Bi}^U (m_{Bi}e_{Bi}\Omega^2 e^{j(\Omega t+\beta_{Bi})}), \end{aligned} \tag{25}$$

$$\begin{aligned} \alpha_1^R &= \sum_{No.(Bi)} \frac{\begin{vmatrix} (t_{11}k_R - t_{14}k_Lk_R - t_{41} + t_{44}k_L) & -(q_{14}^{Bi-N}k_R - q_{44}^{Bi-N}) \\ (t_{31} - t_{34}k_L) & -q_{34}^{Bi-N} \end{vmatrix}}{\begin{vmatrix} (t_{11}k_R - t_{14}k_Lk_R - t_{41} + t_{44}k_L) & (t_{12}k_R - t_{42}) \\ (t_{31} - t_{34}k_L) & t_{32} \end{vmatrix}} (m_{Bi}e_{Bi}\Omega^2 e^{j(\Omega t+\beta_{Bi})}) \\ &= \sum_{No.(Bi)} c_{Bi}^{\alpha} (m_{Bi}e_{Bi}\Omega^2 e^{j(\Omega t+\beta_{Bi})}). \end{aligned} \tag{26}$$

The state vector at the measuring plane of node number Mi is expressed as follows:

$$\{\ \}_{Mi}^M = Q^{1-Mi}\{\ \}_1^R + \sum_{No.(Bi)} Q^{Bi-Mi}\{\ \}_{Bi}. \tag{27}$$

The summation on the right-hand side of Eq. (27) is effective for the unbalance (or balancing) planes only having the node number smaller than the node number of the measuring plane, i.e., for $Bi < Mi$.

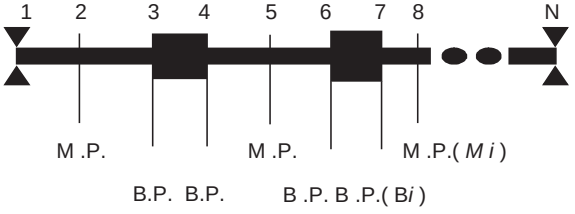

Fig. 8. General rotor model.

The displacement U_{Mi} at the measuring plane is extracted from Eq. (27) as follows:

$$U_{Mi} = \sum_{No.(Bi)} \{(q_{11}^{1-Mi} - q_{14}^{1-Mi}k_L)c_{Bi}^{U} + q_{12}^{1-Mi}c_{Bi}^{\alpha} + q_{14}^{Bi-Mi}\}(m_{Bi}e_{Bi}\Omega^2 e^{j(\Omega t+\beta_{Bi})}). \tag{28}$$

The displacement at the measuring plane is calculated using Eq. (28). The terms $\{(q_{11}^{1-Mi} - q_{14}^{1-Mi}k_L)c_{Bi}^{U} + q_{12}^{1-Mi}c_{Bi}^{\alpha} + q_{14}^{Bi-Mi}\}$ in the right-hand side of the equation are the influence coefficients, which indicate the relation between the displacement at Mi plane and the unbalance at Bi plane. The term q_{14}^{Bi-Mi} in Eq. (28) is effective only when $Bi < Mi$.

4. Simulation

A simplified model is used for calculating the influence coefficients. It has a thick cylinder at mid-span as shown in Fig. 9. The diameters of the left- and right-hand side shafts are 5 and 3 cm, respectively, the length of both shafts is 30 cm. Both the diameter and thickness of the thick cylinder are 10 cm. The rotor is mounted on the resilient bearings at each end.

The elasticity and density of the rotor material are given as $2.12 \times 10^6\ \mathrm{kg_f/cm^2}$ and $0.0078\ \mathrm{kg/cm^3}$, respectively. In the analysis the cylinder element at mid-span is considered as a flexible shaft element having the balancing planes at its ends. The stiffness of the bearings is $1.0 \times 10^{10}\ \mathrm{N/m}$.

Expressing the responses at the measuring planes 2 and 5 in terms of the unbalances at nodes 3 and 4, we have

$$\begin{pmatrix} U_2 \\ U_5 \end{pmatrix} = \begin{bmatrix} \alpha_{23} & \alpha_{24} \\ \alpha_{53} & \alpha_{54} \end{bmatrix} \begin{pmatrix} m_3e_3\Omega^2 e^{j(\Omega t+\beta_3)} \\ m_4e_4\Omega^2 e^{j(\Omega t+\beta_4)} \end{pmatrix}. \tag{29}$$

The influence coefficients α_{23}, α_{24}, α_{53} and α_{54} are calculated using Eq. (28) and shown in Figs. 10–13. The dotted lines indicate the calculations using the finite element method based on Timoshenko beam theory. The influence coefficients obtained by using the method of this research and those obtained using the finite element method show the same trend, though they give the different values in detail. The first four critical speeds are 608.7, 4550.3, 7952.6 and 17 707.4 rad/s when using the present analysis model, and 608.9, 4597.3, 8118.6 and 19 343.1 rad/s when using the finite element method, respectively. The finite element method gives higher values in critical speed calculations. The phenomena have already been shown in the calculation of natural frequencies for the given rotating speeds: the discrepancy appears more significantly for higher modes [1].

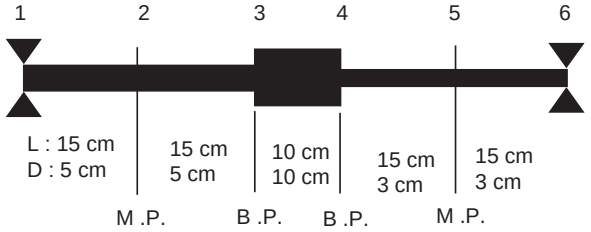

Fig. 9. Simulation model.

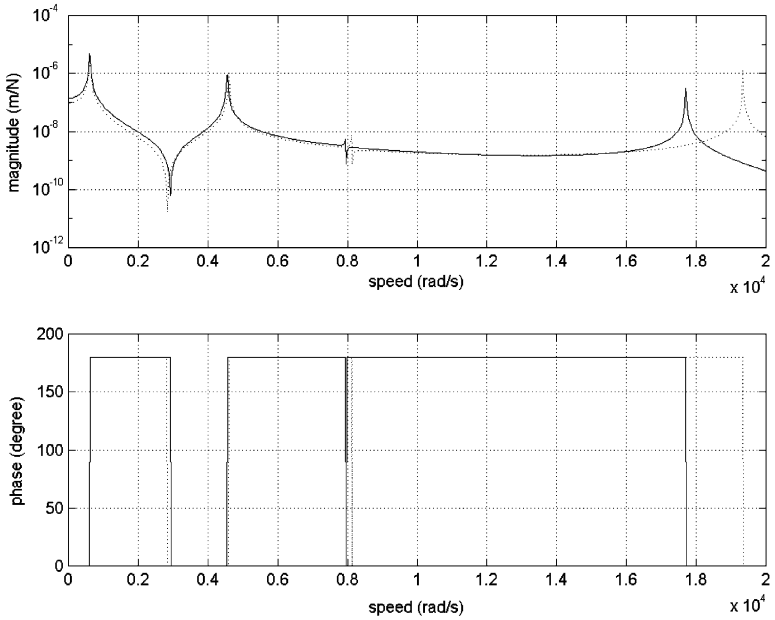

Fig. 10. Influence coefficient α_{23} (solid line: using the transfer matrix method, dotted line: using the finite element method).

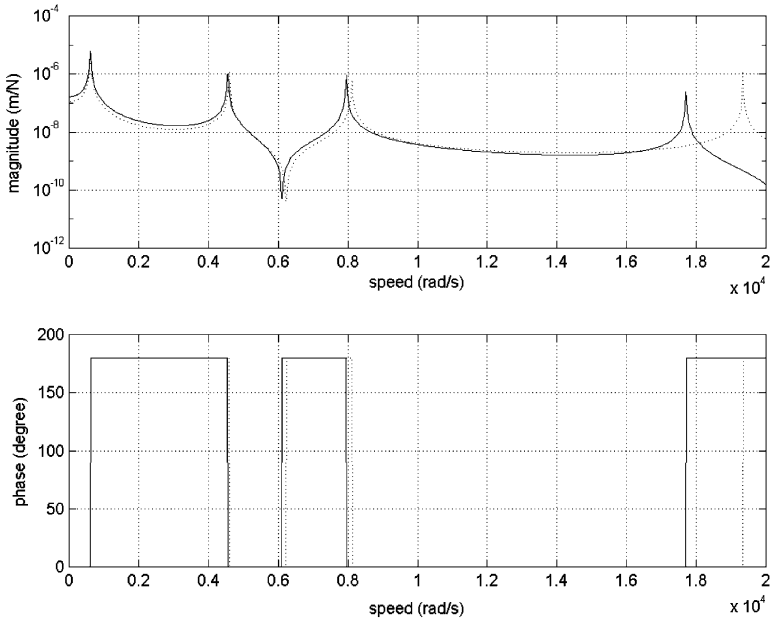

Fig. 11. Influence coefficient α_{24} (solid line: using the transfer matrix method, dotted line: using the finite element method).

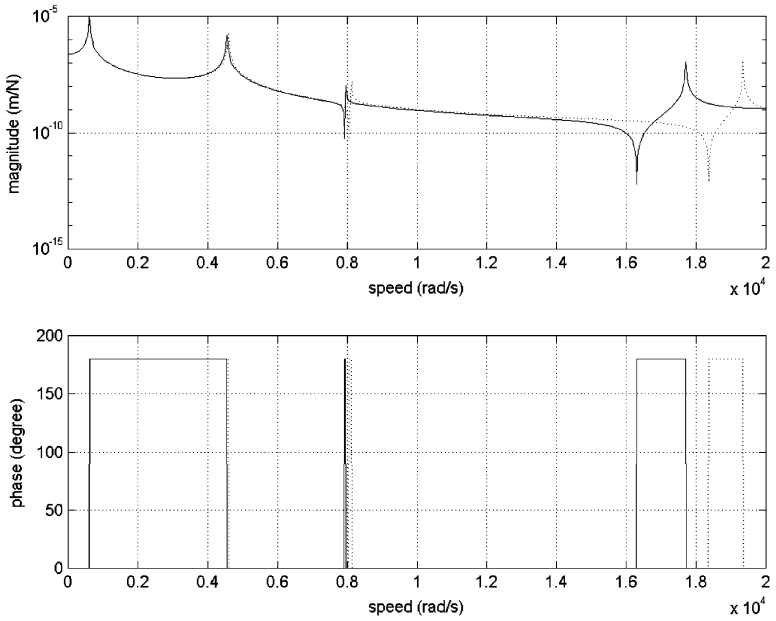

Fig. 12. Influence coefficient α_{53} (solid line: using the transfer matrix method, dotted line: using the finite element method).

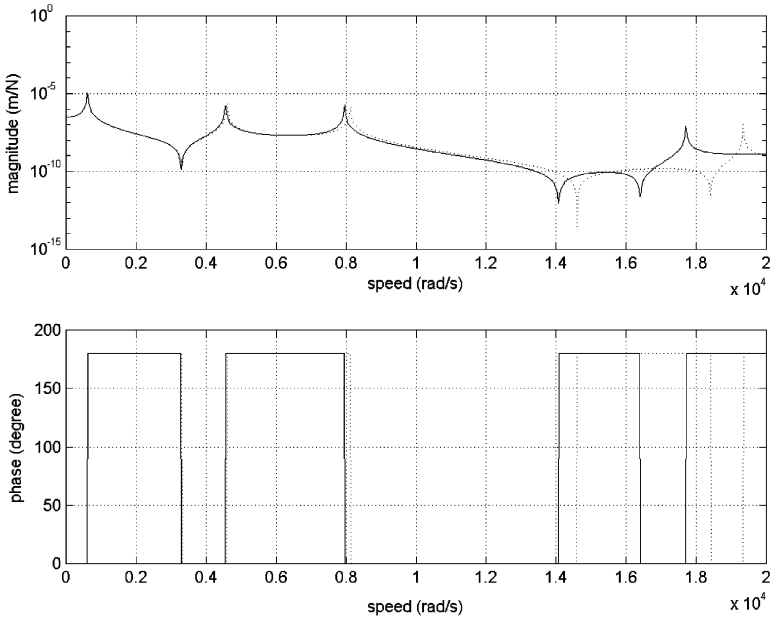

Fig. 13. Influence coefficient α_{54} (solid line: using the transfer matrix method, dotted line: using the finite element method).

The damping is not considered for this calculation because it is included when modelling the disk element and this example does not use the disk element.

It is worth while to note that the anti-resonant frequencies exist between the first and second critical speeds on the influence coefficients, α_{23} and α_{54}. This is because the first and second modes interfere destructively at the frequency. The measuring (output) planes are on the same side with the balancing (input) planes. This shows the trend similar to that the driving-point frequency–response function has an anti-resonance between the first and second resonant frequencies [7]. The anti-resonant frequencies on α_{23} and α_{54}, however, are different from each other because of the different measurement position. On the other hand, the anti-resonant frequency between the two critical speeds does not exist on the influence coefficients, α_{24} and α_{53}.

Similar phenomena due to mode interference are also shown at other frequency ranges. The mass attached on that plane near the anti-resonant frequencies has little effect on the response at the plane. The influence coefficients is too insensitive to use for balancing in such frequency ranges.

Fig. 14 reveals that the third critical speed peak does not appear clearly in the influence coefficients α_{23} and α_{53} of Figs. 10 and 12. The position of balancing plane at node 3 of the analysis model coincides with a nodal point of the third bending mode, thus the mass at the position does little affect the responses.

Fig. 15 shows the influence coefficients α_{23} for the various bearing stiffnesses. The solid line and dash–dot line are shown like a single line in the figure. This shows that the high stiffness bearing does not change significantly the vibration characteristics. The low stiffness models are introduced to simulate the foil and journal bearings: 1×10^6 N/m for the foil bearing and 1×10^8 N/m for the journal bearing.

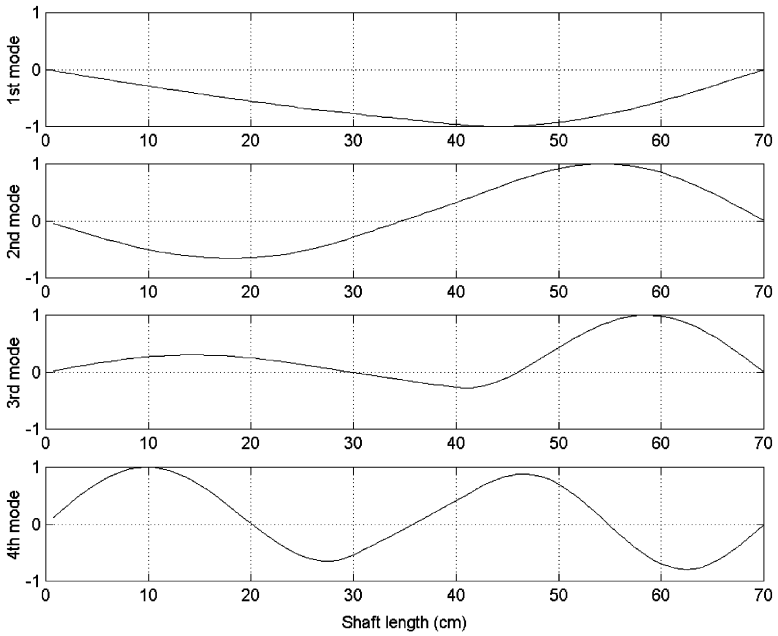

Fig. 14. First four bending vibration modes.

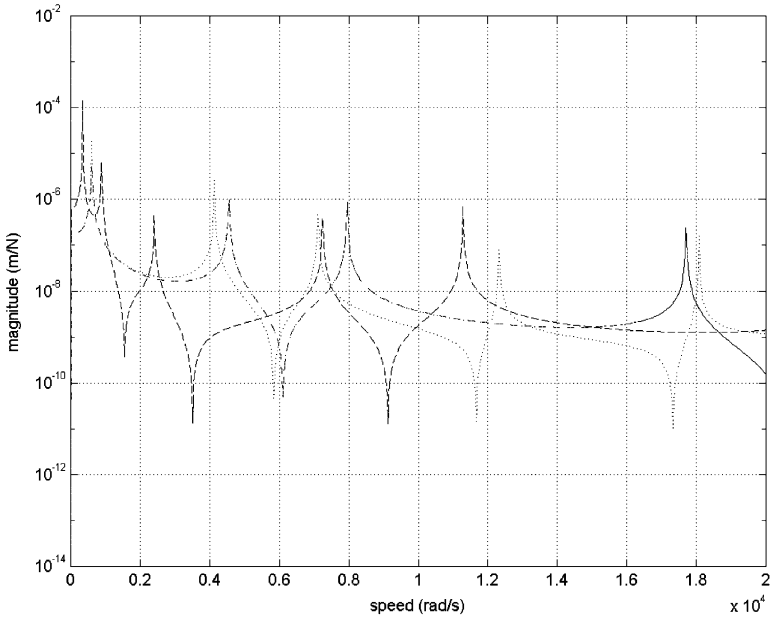

Fig. 15. Influence coefficient α_{24} for various spring stiffness (dashed: 1×10^6 N/m, dotted: 1×10^8 N/m, solid: 1×10^{10} N/m and dash-dot: 1×10^{12} N/m).

5. Conclusions

Complex transfer matrix relating the variables at each end of the elastodynamic shaft element has been derived. The rotary inertia, shear deformation and gyroscopic effects are considered in modelling.

Influence coefficient has analytically been derived for the general flexible rotor having two resilient bearings at both ends. Given are specifications such as material properties, dimensions of rotor, bearing stiffness and the information of positions of the balancing planes and measuring points, the magnitude and phase of the influence coefficients became to be predictable.

Simulations using the proposed method have been compared to the results using the finite element method. They showed very similar trends. Since the present method has straightforwardly been derived from the equation of motion and been expressed in the closed and general form, the exact estimations are expected.

The calculation results show that for the given measuring and balancing planes, some attention shall be given when the rotation speed is chosen. Correction mass does not affect on the balancing procedure near the anti-resonant frequency region because of the insensitiveness of the influence coefficient. Prediction of influence coefficients is recommended, if available.

Acknowledgements

The author thanks Prof. S.W. Hong of Kumoh National University Technology for his helpful FEM analysis.

References

[1] O.S. Jun, J.O. Kim, Free bending vibration of a multi-step rotor, *Journal of Sound and Vibration* 224 (4) (1999) 625–642.
[2] M.S. Darlow, *Balancing of High-Speed Machinery*, Springer, Berlin, 1988.
[3] International Organization for Standardization, Mechanical Vibration—Balance Quality Requirements of Rigid Rotors—Part 1: Determination of Permissible Residual Unbalance, ISO 1940–1, 1986.
[4] International Organization for Standardization, Mechanical Vibration—Methods and Criteria for the Mechanical Balancing of Flexible Rotors, ISO 11342, 1998.
[5] C.-W. Lee, *Vibration Analysis of Rotors*, Kluwer Academic Publishers, The Netherlands, 1993 Chapter 8.
[6] W.H. Beyer, *CRC Standard Mathematical Tables*, CRC Press, Boca Raton, FL, USA, 1979.
[7] International Organization for Standardization, Vibration and Shock—Experimental Determination of Mechanical Mobility—Part 2: Measurements Using Single-point Translational Excitation with an Attached Vibration Exciter, ISO 7626-2, 1990.